In Situ Infrared Observation of a Photo-Decomposition Process of Organic Contaminants on a TiO2 Nanotube Film Surface

著者	Teng Ma, Yasuo Kimura, Daisuke Tadaki, Ayumi Hirano Iwata, Michio Niwano
journal or publication title	Journal of The Electrochemical Society
volume	166
number	15
page range	H842-H848
year	2019-11-18
URL	http://hdl.handle.net/10097/00130723

doi: 10.1149/2.1151915jes

In-situ infrared observation of a photo-decomposition process of organic contaminants on a TiO_2 nanotube film surface

Teng Ma,[1,2,=] Yasuo Kimura,[3,=] Daisuke Tadaki,[4] Ayumi Hirano-Iwata,[1,4] Michio Niwano[4,†,Z]

[1]WPI-Advanced Institute for Materials Research, Tohoku University, 2-1-1 Katahira, Aoba-ku, Sendai 980-8577, Japan
[2]Core Research Cluster, Tohoku University, 2-1-1 Katahira, Aoba-ku, Sendai 980-8577, Japan
[3]Department of Computer Science, Tokyo University of Technology, 1404-1 Katakura-machi Hachioji, Tokyo 192-0914, Japan
[4]Research Institute of Electrical Communication, Tohoku University, 2-1-1 Katahira, Aoba-ku, Sendai 980-8577, Japan

[=]These authors contributed equally to this work
[z]Corresponding Author E-mail Address [niwano@riec.tohoku.ac.jp]
†Present address: Kansei Fukushi Research Institute, Tohoku Fukushi University, Kunimigaoka, Aoba-ku, Sendai 989-3201, Japan

Abstract

We investigated a photocatalytic reaction on TiO_2 nanotube (NT) surfaces using infrared absorption spectroscopy with multiple-reflection geometry (MIR-IRAS). We used an anodization technique to form a film of well-aligned TiO_2 NTs on the Si prism used for MIR-IRAS measurements. The photocatalytic decomposition process of the endocrine disruptor, dioctyl phthalate (DOP), on the TiO_2 NT surface was monitored in-situ and in real time. We demonstrated that the photocatalytic decomposition of organic materials is promoted with the presence of molecular oxygen. It was observed that the amount of surface-adsorbed water molecules changed during the reaction. We proposed a simple reaction model that can reproduce the time-dependent change of the surface coverage of water and DOP. By comparing the photodecomposition of organic materials on TiO_2 NT films with that on TiO_2 nanoparticle (NP) films, we showed that TiO_2 NT films are superior in photocatalytic reactivity compared to NP films. We suggest that the NT structure provides wider and shorter paths for the transport of photo-generated radicals and byproducts, leading to a higher reactivity compared to TiO_2 NPs.

Introduction

Since the first application of the TiO_2 photocatalytic effect by Fujishima *et al*, this unique effect has attracted a lot of attention from both researchers and engineers.[1] Recently, the applications of TiO_2-photocatalysts, such as the photo-oxidation of surface contaminants and photo-reduction for fuel production, have demonstrated strong potential and remarkable progress.[2-13] The nanostructure of the TiO_2 material can substantially affect the photocatalytic efficiency. Salmasi *et al.* has reported that TiO_2 nanotubes (NTs) are superior in reactivity compared to TiO_2 nanoparticles (NPs) as a catalyst of an oxide-sulfurization process.[9] Liu *et al.* has also demonstrated that TiO_2 NTs can oxidize methylcyclonhexane faster than TiO_2 NPs.[11] However, the influence of the nanostructure on the photocatalytic reaction on TiO_2 surfaces has not been well studied.

The first stage of photo-oxidation of organic materials on TiO_2 surfaces is when electron/hole pairs are generated by photons, which are absorbed by the TiO_2 photocatalyst. The holes can react with the surface groups of TiO_2 or water molecules to form hydroxyl radicals ($^\bullet OH$). In particular, surface-bound hydroxyl radicals ($Ti\text{-}^\bullet OH$) are thought to play an important role in oxidizing organic species near the TiO_2 surface.[15] On the other hand, the photo-generated electrons in bulk TiO_2 may react with O_2 to form $^\bullet O_2^-$ radicals, which also participate in the photo-induced decomposition process of the surface organic materials.[15,16] Henderson showed that the photo-induced oxygen atoms exchange between the TiO_2 and gaseous O_2 under vacuum conditions.[17] It has also been reported that water molecules can incorporate into a TiO_2 lattice during the photocatalytic reaction.[5] It seems that water molecules and molecular oxygen (O_2) can both act as the source of the oxygen atoms which are required for the photo-oxidation reaction. However, there is seldom any study comparing the reactivity of H_2O and O_2 in a photo-induced reaction in detail, especially on TiO_2 NT surfaces.

In this study, therefore, we investigated the photocatalytic reaction at TiO_2 NT surfaces using infrared absorption spectroscopy with multiple-reflection geometry (MIR-IRAS). This provided us with valuable information on the chemical changes on the molecular scale relevant to the surface reactions.[6,18-20] In order to carry out MIR-IRAS measurements on TiO_2 NT film surfaces, we needed to form a TiO_2 NT film on an MIR Si prism surface. The conventional method for forming vertically aligned TiO_2 NT arrays is to anodize metallic Ti plates which are infrared opaque.[7,10,14] We therefore developed a method to fabricate TiO_2 NTs directly on the Si MIR prism. Using the endocrine disrupting chemical, dioctyl phthalate (DOP), as a model organic material, we studied the photocatalytic process of organic materials on TiO_2 NT surfaces in different reaction environments to demonstrate the effect of water and oxygen on photocatalysis. Also, we investigated the photocatalytic reaction of both TiO_2 NPs and NTs to show how the nanostructure affects the photo-oxidation reaction.

Experimental

A. Experimental setup

The experimental setup we used in this study is shown schematically in Fig. 1. The Si prism was mounted in a specially designed cell, as shown in Fig. 1. In the sealed cell, we can precisely control the humidity and composition of the gas. In order to investigate the photocatalytic reaction of TiO_2, three ultraviolet (UV) light-emitting diodes (LED, 365 nm) were attached to the top cover (acrylic) of the cell. 60 µL of DOP in ethanol solution (100 µM) was dispersed on the TiO_2 NT film surface. After fully evaporating the ethanol from the TiO_2 surface, the Si prism was transferred into the cell shown in Fig. 1. The humidity and the temperature (25 °C) in the cell were precisely controlled to obtain reproducible data. We investigated the photocatalytic process in dry (relative humidity, RH = 3–7%) and wet conditions (RH = 60–65%) with two different carrier gases, Air and pure N_2 gas. It should be noted that the air contained 20 % oxygen. The decomposition of DOP on TiO_2 NPs and NTs under UV illumination was monitored in-situ using MIR-IRAS. An infrared beam entered the Si prism through one side of the beveled edges and was collected at the other side of the bevels using a liquid-nitrogen-cooled mercury-cadmium-telluride (MCT) detector. In the prism, the beam reflected about 100 times generating an evanescent field at the surface. The evanescent field is highly sensitive to chemical changes, therefore it is suitable for the in-situ observation of the photocatalytic reaction which happens on the TiO_2 surface.

B. Si Prism fabrication for MIR-IRAS

The fabrication process of the Si prism for MIR-IRAS is shown in Fig. 2. A highly doped silicon prism (10 × 4 × 0.5 mm^3) with 45° beveled edges was cleaned in a mixture of H_2SO_4 and H_2O_2, followed by 5% hydrofluoric acid. A thin layer of Au was deposited onto the backside of the Si prism by thermal evaporation through a metal mask. After that was done, 50 nm of TiO_2 and 200 nm of Ti were sequentially deposited onto the surface of the prism. Then the TiO_2 NTs were formed by anodizing the deposited Ti layer. The detailed fabrication method for the TiO_2 NTs has been described elsewhere.[14,22] The Au layer at the bottom of the prism acted as the contact for the anodization process. The as-formed TiO_2 NTs were then crystallized (anatase) at 450 °C to achieve the high catalytic activity.[21] Figures 3(a) and 3(b) show typical top and cross-sectional views of the scanning electron microscopy (SEM) images of the TiO_2 NT film fabricated on the Si MIR prism. The SEM images were recorded at an accelerating voltage of 3.0 kV using Hitachi SU-8000 equipment. Fig. 3 shows that the inner and outer diameters of the TiO_2 NTs were about 50 and 100 nm, respectively. The thickness of the film was approximately 500 nm. It is known that TiO_2 in the anatase form exhibits high photocatalytic activity under ultraviolet (UV) illumination. TiO_2 NT films grown by anodization of metallic Ti is amorphous and can be converted to the anatase form by annealing at approximately 450 °C. Fig. 3(c) shows a typical X-ray diffraction (XRD) pattern of the TiO_2 NT film post annealing. XRD measurements were performed using Rigaku RINT-2000 equipment with CuKα radiation operating at 40 kV and 40 mA. The scanning step was 0.02°. It can be seen in Fig. 3(c) that the as-formed TiO_2 NT film was transformed into the anatase phase due to post annealing at 450 °C in air.

To fabricate the prism with the TiO_2 NPs, a thin layer of TiO_2 NPs (anatase, Solaronix) was spin-coated from an aqueous suspension (2.5 g/mL). The thickness of the NP film was similar to that of NT film (500 nm). The NP film was then annealed at 450 °C to improve adhesion between the prism and the NP layer.

Results and discussion

A. Reaction-atmosphere-dependence of photocatalytic decomposition of organic materials

In Fig. 4 we have shown the IRAS spectrum of DOP on the TiO_2 NT film after UV irradiation. The reference for this spectra was the spectrum of the as-deposited DOP on the TiO_2 NT surface prior to UV illumination, which we have shown in the bottom of Fig. 4. The molecular structure of DOP is shown in the inset of Fig. 4. Two distinct features can be identified at around 1705 and 2800–3000 cm^{-1}. The feature at 1705 cm^{-1} represents the C=O stretching modes of ester groups, and the feature at 2800–3000 cm^{-1} represents the C-H stretching vibrational modes of $-CH_3$, $-CH_2$ and -CH groups in the DOP molecule. It can be seen in Fig. 4 that the IRAS spectrum under UV illumination exhibits troughs, the positions of which are the same as those of the dominant vibrational modes of the pristine DOP. This clearly indicates that due to UV illumination, the DOP molecules on the TiO_2 NT film were decomposed. As described later, we observed that DOP on the bare Si surface did not show any spectral changes under UV illumination. Thus, we concluded that the DOP decomposition observed on the TiO_2 NT film is due to the photocatalytic effect of the TiO_2 NTs.

The primary purpose of this study was to clarify the dependence of photocatalytic effect on the reaction atmosphere. Therefore, we examined photocatalytic reactions under the following four types of environments: (1) dry air, (2) pure nitrogen gas, (3) humidified air and (4) humidified nitrogen gas. Humidity control was performed by controlling the gas flow rate as the gas was supplied to the measurement cell through a bubbler. The humidity of the dry atmosphere (dry condition) was set at 3–7%, and that of the humidified atmosphere (wet condition) was RH = 60–65%. Fig. 5 shows the spectral changes on TiO_2 NT film surfaces under UV illumination in the four different environments. From Fig. 5, it can be seen that the decomposition of DOP proceeds faster in oxygen-containing dry air than in oxygen-free nitrogen gas. Also, it appears that the humidity does not significantly promote DOP decomposition.

In order to further investigate how the photocatalytic reaction proceeds at the TiO_2 surface, we have looked in detail at the spectral changes in the wavenumber region between 2500 and 4000 cm^{-1}, where the C-H and O-H stretching vibrational modes should appear. To quantify the decomposition rate of the DOP molecules under UV illumination, we focused on the negative feature observed at a wavenumber of 2964 cm^{-1} (Fig. 5). This feature corresponded to the C-H stretching vibrations of DOP, and its peak intensity represented the amount of DOP decomposed and detached from the TiO_2 NT surface. We calculated the DOP residue ratio based on the peak intensities at 2964 cm^{-1} (as seen in Fig. 5) and the same peak before UV illumination. The time evolution of the DOP residue ratio for the four different environments (dry air, pure N_2, humidified air and humidified N_2) is shown in Fig. 6. For comparison, the result obtained for a bare Si surface is also shown in Fig. 6. The calculated DOP residue ratio hardly changed during UV illumination when DOP was deposited on the Si prism surfaces. It is evident that the residue ratio significantly changed when DOP was deposited on the TiO_2 NT film surface. These facts suggest that DOP decomposition is induced by the photocatalytic effect of the TiO_2 NTs upon UV illumination. We also noticed that the reaction rate of the DOP decomposition on the TiO_2 NT surface depends on the atmosphere. In a N_2 atmosphere, only 40% of the DOP molecules were decomposed in 5 hours of UV illumination, while the decomposition ratio increased to 80% in the oxygen-containing atmospheres. Furthermore, we observed that the decomposition ratio does not depend on the humidity of the atmosphere. These observations indicate that O_2 is superior in promoting the photo-oxidation reaction on TiO_2 NT surfaces compared to N_2 and H_2O. The oxygen molecules react with photo-generated electrons to form ${}^{\bullet}O_2^-$ radicals, which may further react with and decompose organic molecules on the surface. This then produces carbon dioxide as the final product.[15,16] In addition, the oxygen molecules may also assist the consumption of photo-generated electrons and prevent the electron/hole recombination, leading to an enhancement of the photocatalytic effect.

B. Time-dependent surface coverage of water

In order to understand how water is involved in the photocatalytic reaction, we looked at the IR spectra in the range of 3000–4000 cm^{-1}, where the O-H stretching mode (3400 cm^{-1}) of water appears. As shown in Fig. 5, in all of the tested atmospheres, the amount of H_2O adsorbed at the TiO_2 surface initially decreased with illumination time. Since we purged the sample cell with dry N_2 before starting the UV illumination, the observed loss of water at the surface is not due to the evaporation of H_2O from the surface. Almost all of loosely bound H_2O molecules should have been removed from the surface during purging process. The remaining H_2O molecules would be strongly adsorbed to the TiO_2 surface.[23] The reduction of H_2O molecules at the surface during UV illumination, as shown in Fig. 5, indicates that the H_2O molecules present at the TiO_2 surface are partially involved in the photocatalytic reaction, as has been previously suggested by Montoya *et al.*,[5] who reported that H_2O can act as an oxidation reagent in the photo-oxidation process in aqueous solutions. However, as can be seen from Fig. 6, an increase in the humidity of the atmosphere did not facilitate the decomposition of DOP.

In Fig. 7, we show the plot of the time dependence of the absorbance of the O-H vibrational mode along with that of the C-H vibrational mode. The initial decrease observed for all the atmosphere types can be attributed to the removal of surface water by the photocatalytic effect of the TiO_2 surface. In the humidified atmosphere, in particular in wet air, an increase in the intensity of OH band was observed. The subsequent increase is attributed to the adsorption of water on the exposed TiO_2 surface after the decomposition of the DOP molecules. It has been reported that the TiO_2 surface becomes hydrophilic after the removal of surface contaminants by the photocatalytic reaction due to the replenishment of surface hydroxyl groups.[24] This means that after removing surface contaminants, the water molecules in the atmosphere most likely get adsorbed onto the surface.

To support our interpretation, we propose a simple model to simulate the time evolution of the amount of surface water and DOP. The concept of our model is shown schematically in Fig. 8. Suppose the starting surface is covered with DOP and water. Their relative coverage is represented by θ_{DOP} and θ_{water}, respectively. DOP and water are decomposed and removed from the TiO_2 NT surface through the photocatalytic reaction. The rate constants for these reactions are k_d^{DOP} and k_d^{water}. After the removal of the surface adsorbate, the surface becomes hydrophilic and the water molecules in the atmosphere readsorb on the surface. The reaction constant of water readsorption is k_{ad}^{water}. In our model, the humidity of the atmosphere is included in this rate constant; in other words, the higher the humidity is, the larger the value of k_{ad}^{water} is. The reaction rate equations representing the temporal change of the surface coverage of water and DOP are as follows:

$$d\,\theta_{DOP}/dt = -k_d^{DOP}\theta_{DOP}\ , \tag{1}$$

$$d\,\theta_{bare}/dt = k_d^{DOP}\theta_{DOP} + k_d^{water}\theta_{water} - k_{ad}^{water}\theta_{bare}\,, \tag{2}$$

$$d\theta_{water}/dt = -k_d^{water}\theta_{water} + k_{ad}^{water}\theta_{bare}. \tag{3}$$

These reaction equations were solved by a sequential calculation method to determine the amount of surface adsorbed water and DOP. The results of calculation are shown in Fig. 9. The parameters which we used in the calculations to obtain a good fit to the experiment are shown in Table I. The initial value of θ_{DOP}, θ_{DOP}^0, was set at the same value. The initial value of θ_{water}, θ_{water}^0, was adjusted to reproduce the variation of the absorbance of the O-H vibrational mode. It should be noted that, as mentioned above, θ_{DOP} and θ_{water} are relative surface coverage, and therefore the sum of θ_{DOP}^0 and θ_{water}^0 is not unity. It can be seen from Fig. 9 that the calculation quantitatively reproduces the experimental results shown in Fig. 7, indicating that our assumption on the temporal change of water adsorption is reasonable. From the parameter values shown in Table I, several points are worth mentioning. Firstly, the decomposition rate of water is about an order of magnitude larger than that of DOP. This is quite natural considering that the decomposition of the water molecule is a single-step process while the thorough decomposition of DOP requires multiple reactive radicals and it is a multi-steps process. Secondly, the decomposition rate of DOP is larger in the oxygen-containing atmosphere than that in the oxygen-free atmosphere. This result is consistent with our conclusion from Fig. 5 and Fig. 6, which is that oxygen is more effective in facilitating the photocatalytic reaction on the TiO_2 NT surface. Thirdly, the readsorption rate in the humidified atmosphere is larger than that in the dry atmosphere. This may be attributed to the increase in the impinging rate of water molecule on the surface in the humidified ambient. Finally, it should be noted that the readsorption rate in the oxygen-containing atmosphere is larger than that in the corresponding oxygen-free atmosphere. This could be attributed to the higher decomposition rate of DOP in oxygen-containing atmosphere, and thus larger surface area for water adsorption.

Close inspection of Fig. 5 reveals that the peak at 3740 cm^{-1}, as indicated by arrows in Figs. 5(a) and 5(b), shows up on the surface in the O_2-containing atmosphere. On the other hand, no peaks can be identified in the vicinity of 3740 cm^{-1} on the TiO_2 surface in the oxygen-free atmosphere. This peak is attributed to the O-H stretching vibration mode of the surface Ti-OH species on TiO_2. We suppose that removal of DOP and water molecules produces Ti-OH species on the resulting bare TiO_2 surface. Note that such a surface will be hydrophilic and therefore easy to adsorb water. Accordingly, we interpret that the preferential formation of surface Ti-OH species in the oxygen-containing atmosphere is the origin for the observed enhancement of water readsorption on the surface. We believe that oxygen radicals would favorably create surface Ti-OH species. However, the details why the surface Ti-OH species are favorably formed in the O_2-containing atmosphere are not clear at the present moment.

C. Comparison of NT and NP films

In order to investigate how the nanostructure affects the photocatalytic reaction, we fabricated a Si MIR prism with a thin layer of TiO_2 NPs. As shown in Fig. 10, a thin mesoporous film of NPs with a size of 15~20 nm formed on the Si MIR prism, which is in contrast to the structure of the NT thin films where the nanotubes were regularly aligned. In Fig. 11, we showed a series of IRAS spectra of DOP on the TiO_2 NP film upon UV illumination in dry air. These spectra have been collected for different illumination durations and the spectrum of the DOP on the TiO_2 NP surface before UV illumination was used as the reference. It can be seen by comparing Figs. 4 and 11 that the spectral changes observed for the NP TiO_2 are quite similar to those observed for the NT TiO_2 film. The two intense features observed around 1705 cm^{-1} and 2800~3000 cm^{-1}, are due to the C=O stretching modes of the ester groups and the C-H stretching modes of the $-CH_3$, $-CH_2$ and -CH groups in the DOP molecule, respectively.

To compare the photocatalytic reactivity of the TiO_2 NTs and NPs, we examined the time-evolution of the DOP residual ratio for the TiO_2 NT and NP films in Fig. 12. We can see from Fig. 12 that the photocatalytic decomposition of DOP on the TiO_2 NT and NP surfaces proceeded in a similar fashion for the first hour of UV illumination. However, the reaction rate on the TiO_2 NPs slowed down afterwards. After 5 hours of UV illumination, only half of the DOP molecules were decomposed. On the other hand, the DOP molecules on the TiO_2 NTs kept being decomposed even after 5 hours of illumination. Despite a larger surface area, the NP film seems to exhibit a lower photocatalytic reactivity than the NT film. Because both of the NTs and NPs were crystalized in the anatase phase, the only difference is their nanostructure. As described above, we believe that the oxygen radicals are favorably formed in an oxygen atmosphere to promote the decomposition of organic materials. In the case of the NT film, the straight pores are oriented perpendicular to the film surface, which may facilitate the penetration of oxygen and the desorption of the decomposed products, and thus promote the decomposition of organic materials. Furthermore, the longer charge diffusion length in the TiO_2 NTs most probably reduces the possibility of charge recombination at the interface, which leads to highly efficient photodecomposition.[25] A more thorough investigation will be needed to determine which factors play a more important role in improving photocatalytic reactivity.

Conclusions

In this study we have investigated in-situ the photodecomposition process of organic materials on a TiO_2 NT film surface using a MIR-IRAS method. To carry out this study, we fabricated special Si MIR prisms with well-aligned TiO_2 NT films formed on a Si prism surface. To clarify the atmospheric dependence of the photocatalytic reaction, we examined the spectral changes of the TiO_2 NT film surface induced by UV illumination under four different types of atmospheres which were dry air, humidified air, pure N_2 gas, and humidified N_2 gas. Our IRAS data clearly demonstrated that oxygen gas plays an important role in promoting the photocatalytic decomposition of organic materials. We confirmed that the water molecules adsorbed on the TiO_2 surface decompose faster than the organic materials on the surface. In an oxygen-containing atmosphere, the surface Ti-OH species were preferentially generated on the TiO_2 surface after removal of the surface contaminants and water. Finally, we found that the TiO_2 NT films are superior in photo-oxidation reactivity over conventional TiO_2 NP-based films. We suggested that the TiO_2 NT film has a straight path for oxygen adsorption and the release of byproducts and reactive radicals, leading to an enhanced photocatalytic effect.

Acknowledgments

The authors would like to thank Taka-aki Miya and Dr. Ryota Kojima for their technical assistance with the experiments. This research has been partially carried out at the Fundamental Technology Center, Research Institute of Electrical Communication, Tohoku University. This work was partially supported by the CREST program “Development of Atomic or Molecular Two-Dimensional Functional Films and Creation of Fundamental Technologies for Their Applications” (Grant JPMJCR14F3) of the Japan Science and Technology Agency (JST). It was also partially supported by JSPS KAKENHI Grant Number 18K14120.

References

1. A. Fujishima, and K. Honda, Electrochemical Photolysis of Water at a Semiconductor Electrode. *Nature*, **238**, 37-38 (1972).
2. R. Wang, K. Hashimoto, A. Fujishima, M. Chikuni, E. Kojima, A. Kitamura, M. Shimohigoshi, and T. Watanabe, Light-induced amphiphilic surfaces. *Nature*, **388**, 431–432 (1997).
3. X. Quan, S. Yang, X. Ruan, and H. Zhao, Preparation of Titania Nanotubes and Their Environmental Applications as Electrode. *Environ. Sci. Technol.*, **39** (10), 3770–3775 (2005).
4. C. Liu, A. Zhang, A. Y. Si, D. N. Pei, and H. Q. Yu, Photochemical Anti-Fouling Approach for Electrochemical Pollutant Degradation on Facet-Tailored TiO2 Single Crystals. *Environ. Sci. Technol.*, **51** (19), 11326–11335 (2017).
5. J. F. Montoya, I. Ivanova, R. Dillert, D. W. Bahnemann, P. Salvador, and J. Peral, Catalytic Role of Surface Oxygens in TiO2 Photooxidation Reactions: Aqueous Benzene Photooxidation with $Ti^{18}O_2$ under Anaerobic Conditions. *J. Phys. Chem. Lett.*, **4**, 1415−1422 (2013).
6. A. R. Almeida, J. A. Moulijn, and G. Mul, In Situ ATR-FTIR Study on the Selective Photo-oxidation of Cyclohexane over Anatase TiO_2. *J. Phys. Chem. C*, **112**, 1552-1561 (2008).
7. S. P. Albu, A. Ghicov, J. M. Macak, R. Hahn, and P. Schmuki, Self-Organized, Free-Standing TiO2 Nanotube Membrane for Flow-through Photocatalytic Applications. *Nano*

Lett., **7**(5), 1286-1289 (2007).

8. T. Inoue, A. Fujishima, S. Konishi, and K. Honda, Photoelectrocatalytic reduction of carbon dioxide in aqueous suspensions of semiconductor powders. *Nature*, **277**, 637-638 (1979).
9. M. Salmasi, S. Fatemi, and Y. Mortazavi, Fabrication of promoted TiO2 nanotubes with superior catalytic activity against TiO2 nanoparticles as the catalyst of oxi-desulfurization process. *J. Ind. Eng. Chem.*, **39**, 66-76 (2016).
10. N. Liu, C. Schneider, D. Freitag, U. Venkatesan,V. R. R. Marthala, M. Hartmann, B. Winter, E. Spiecker, A. Osvet, E. M. Zolnhofer, K. Meyer, T. Nakajima, X. Zhou, and P. Schmuki, Hydrogenated Anatase: Strong Photocatalytic Dihydrogen Evolutionwithout the Use of a Co-Catalyst. *Angew. Chem.*, **126**, 14425 –14429 (2014).
11. W. Liu, J. Gao, F. Zhang, and G. Zhang, Preparation of TiO2 Nanotubes and Their Photocatalytic Properties in Degradation Methylcyclohexane. *Mater. Trans.*, **48**(9), 2464-2466 (2007).
12. G. K. Ramesha, J. F. Brennecke, and P. V. Kamat, Origin of Catalytic Effect in the Reduction of CO2 at Nanostructured TiO2 Films. *ACS Catal.*, **4**(9), 3249–3254 (2014).
13. Y. Yan, M. Han, A Konkin, T. Koppe, D. Wang, T. Andreu, G. Chen, U. Vetter, J. R. Morante, and P. Schaaf, Slightly hydrogenated TiO_2 with enhanced photocatalytic performance. *J. Mater. Chem. A*, **2**, 12708-12716 (2014).
14. R. Kojima, Y. Kimura, T. Ma, K. Ishibashi, D. Tadaki, R. A. Rosenberg, A. Hirano-Iwata, and M. Niwano, Fabrication and Characterization of Front-Illuminated Dye-Sensitized Solar Cells with Anodic Titanium Oxide Nanotubes.
J. Electrochem. Soc., **164**(2) H78-H84 (2017).
15. O.Legrini, E.Oliveros, A.M.Braun, Photochemical processes for water treatment. *Chem. Rev.*, **93**, 671-698 (1993).
16. A. Mills, and S. L. Hunte, An overview of semiconductor photocatalysis. *J. Photochem. Photobiol. A*, **108**(1), 1-35 (1997).
17. M. A. Henderson, A Surface Science Perspective on Photocatalysis. *Surf. Sci. Rep.*, **66**, 185-297 (2011).
18. K. Miyamoto, K. Ishibashi, K. Hiroi, Y. Kimura, H. Ishii, and M. Niwano, Label-free

detection and classification of DNA by surface vibration spectroscopy in conjugation with electrophoresis. *Appl. Phys. Letts.*, **86**, 053902 (2005).

19. T. Ma, J. Zhang, R. Kojima, D. Tadaki, Y. Kimura, and M. Niwano, Investigation of TiO_2 Surface Modification with [6,6]-Phenyl-C_{61}-butyric Acid for Titania/Polymer Hybrid Solar Cells. *Jpn. J. Appl. Phys.*, **52**, 112301 (2013).
20. T. Ma, M. Cagnoni, D. Tadaki, A. Hirano-Iwata, and M. Niwano, Annealing-induced chemical and structural changes in tri-iodide and mixed-halide organometal perovskite layers. *J. Mater. Chem. A*, **3**, 14195-14201 (2015).
21. T. Luttrell, S. Halpegamage, J. Tao, A. Kramer, E. Sutter, and M. Batzill, Why is anatase a better photocatalyst than rutile? - Model studies on epitaxial TiO_2 films. *Sci. Rep.*, **4**, 4043 (2014).
22. T. Ma, R. Kojima, D. Tadaki, J. Zhang, Y. Kimura, and M. Niwano, Fabrication of polymer/TiO2-nanotube-based hybrid structures using a solvent-vapor-assisted coating method. *Mater. Res. Express*, **1**, 045048 (2014).
23. S. Hosseinpour, F. Tang, F. Wang, R. A. Livingstone, S. J. Schlegel, T. Ohto, M. Bonn, Y. Nagata, and E. H. G. Backus, Chemisorbed and Physisorbed Water at the TiO2/Water Interface. *J. Phys. Chem. Lett.*, **8**(10), 2195-2199 (2017).
24. N. Sakai, A. Fujishima, T. Watanabe and K. Hashimoto, J. Phys. Chem. B 107, (2003) 1028–1035.
25. J. R. Jennings, A. Ghicov, L. M. Peter, P. Schmuki, and A. B. Walker, Dye-Sensitized Solar Cells Based on Oriented TiO2 Nanotube Arrays: Transport, Trapping, and Transfer of Electrons. *J. Am. Chem. Soc.*, **130**, 13364–13372 (2008).

Tables

Table I. Parameters used for the calculations.

Atmosphere	$\theta_{\mathrm{DOP}}^{0}$	$\theta_{\mathrm{water}}^{0}$	$k_{\mathrm{d}}^{\mathrm{DOP}}$	$k_{\mathrm{d}}^{\mathrm{water}}$	$k_{\mathrm{ad}}^{\mathrm{water}}$
Dried air	1	0.2	0.005	0.05	0.005
Humidified air	1	1	0.005	0.05	0.05
Pure N_2	1	0.5	0.002	0.02	0.0005
Humidified N_2	1	1	0.002	0.02	0.005

Figure Captions

Fig. 1. Experimental setup for the MIR-IRAS measurement.

Fig. 2. Fabrication process of the Si prism with TiO_2 NTs.

Fig. 3. (a) Top view and (b) cross-sectional view of SEM images of the fabricated TiO_2 NT film. (c) Measured (black) and calculated (red) XRD patterns of TiO_2 NTs after post-annealing.

Fig. 4. IRAS spectrum of the DOP deposited on the TiO_2 NTs after UV illumination in dry air. A typical infrared spectrum of DOP on the TiO2 NTs is shown at the bottom of the figure. The inset shows the molecular structure of DOP.

Fig. 5. IRAS spectra of DOP on the TiO_2 NTs during UV illumination in (a) dry air, (b) humidified air, (c) N_2 and (d) humidified N_2 atmosphere. The reference of these spectra is the spectrum of DOP on the TiO_2 NTs before UV illumination.

Fig. 6. Time-evolution of the DOP residue ratio in which the calculation is based on the peak intensities at 2960 cm^{-1} in four types of atmospheres: dry air, humidified air, N_2 and humidified N_2.

Fig. 7. Temporal changes in the absorbance of the C-H stretching vibrational peak at 2960 cm^{-1} and of the O-H stretching vibrational peak at 3400 cm^{-1} for the four different types of atmospheres: dry air, humidified air (a), N_2 and humidified N_2 (b). The absorbance was normalized to that of the corresponding peaks of the as-deposited DOP prior to UV illumination.

Fig. 8. Schematic of a simple model for simulating the time evolution of the surface coverage of water and DOP.

Fig. 9. Calculated time evolution of the surface coverage of water and DOP obtained for the different types of atmospheres.

Fig. 10. Top and side views of the SEM images of the TiO_2 NP film.

Fig. 11. IRAS spectra of DOP on the TiO_2 NP film during UV illumination in dry air. The reference of these spectra is the spectrum of DOP on the as-formed TiO_2 NP film before UV illumination.

Fig. 12. Time-evolution of DOP residue ratios on the TiO_2 NT and NP films in dry air. The residue ratios were calculated based on the peak intensity at 2960 cm^{-1}.

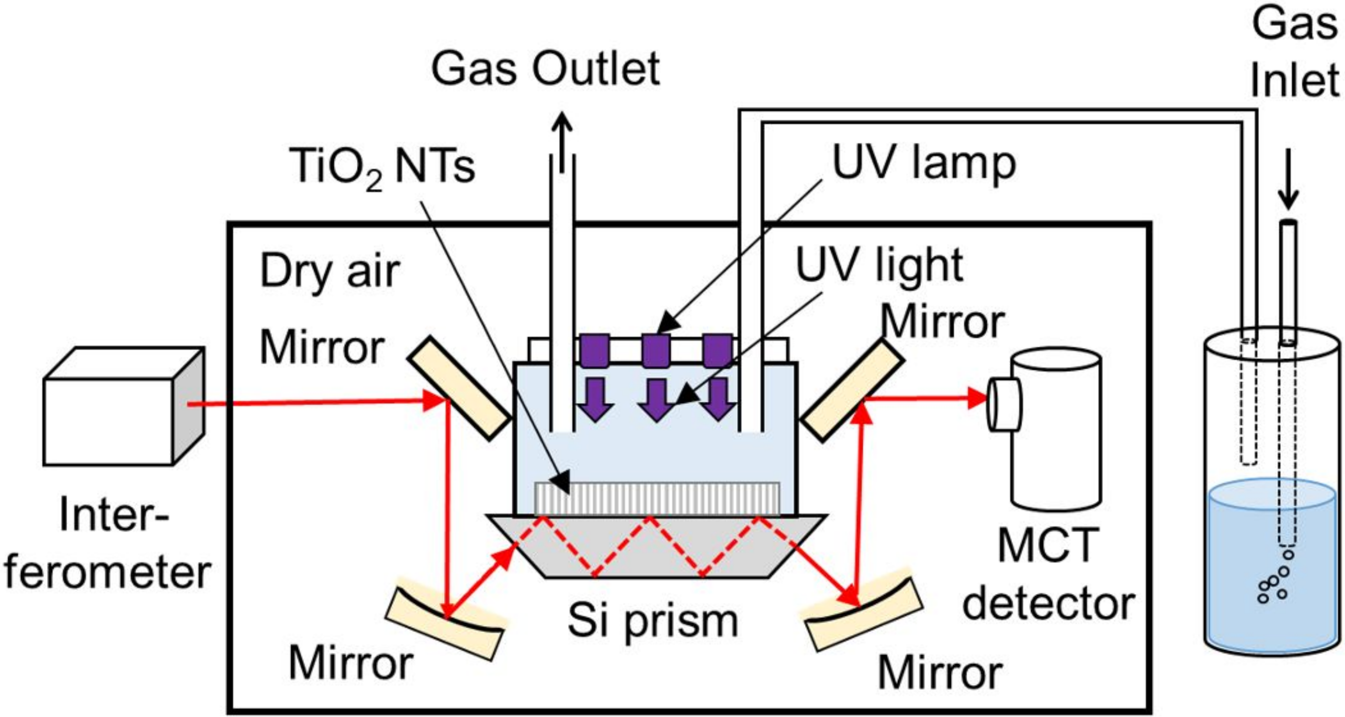
Gas Outlet
Gas Inlet
TiO₂ NTs
UV lamp
UV light
Dry air
Mirror
Mirror
Inter-ferometer
MCT detector
Si prism
Mirror
Mirror

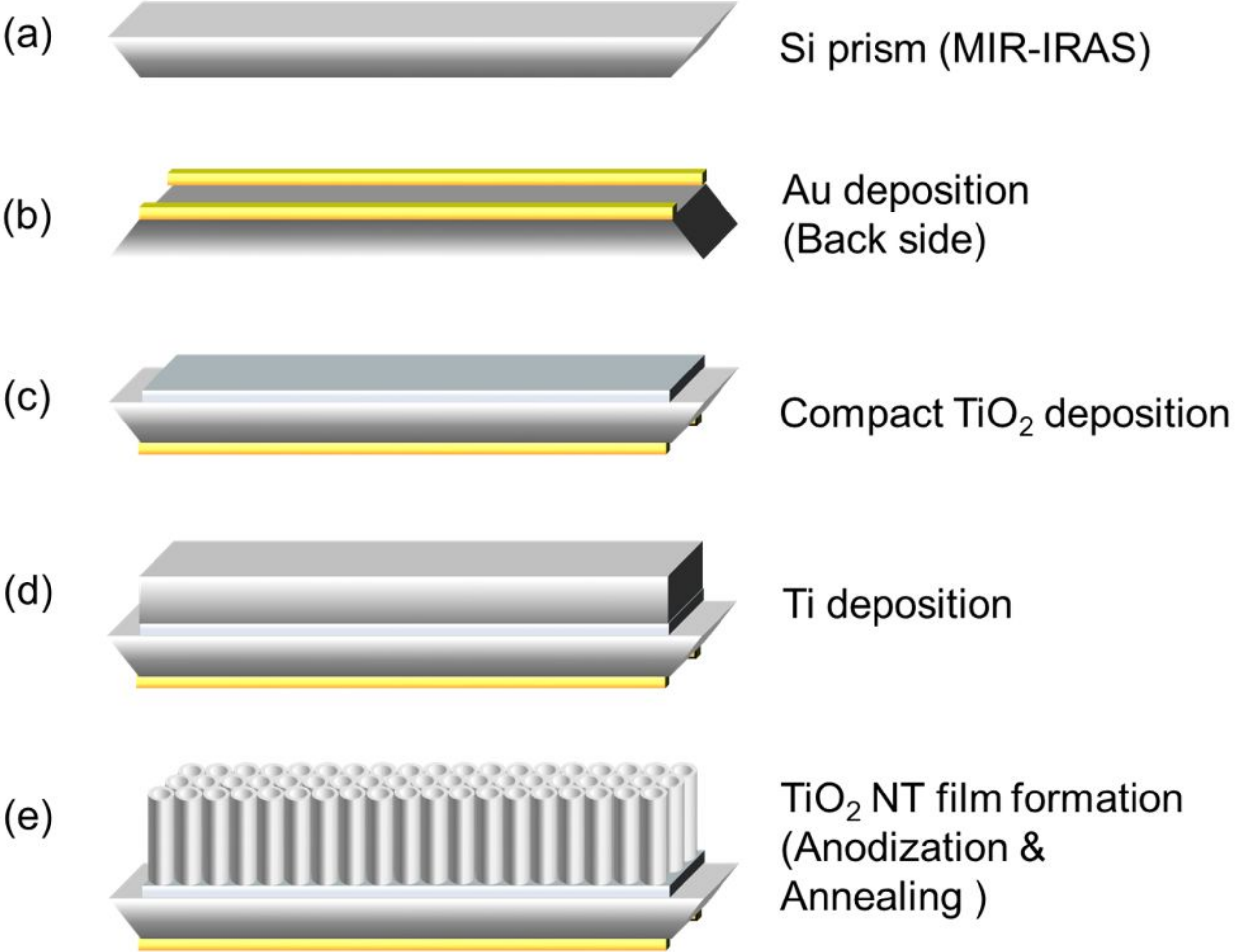
(a)
Si prism (MIR-IRAS)
(b)
Au deposition
(Back side)
(c)
Compact TiO_2 deposition
(d)
Ti deposition
(e)
TiO_2 NT film formation
(Anodization &
Annealing)

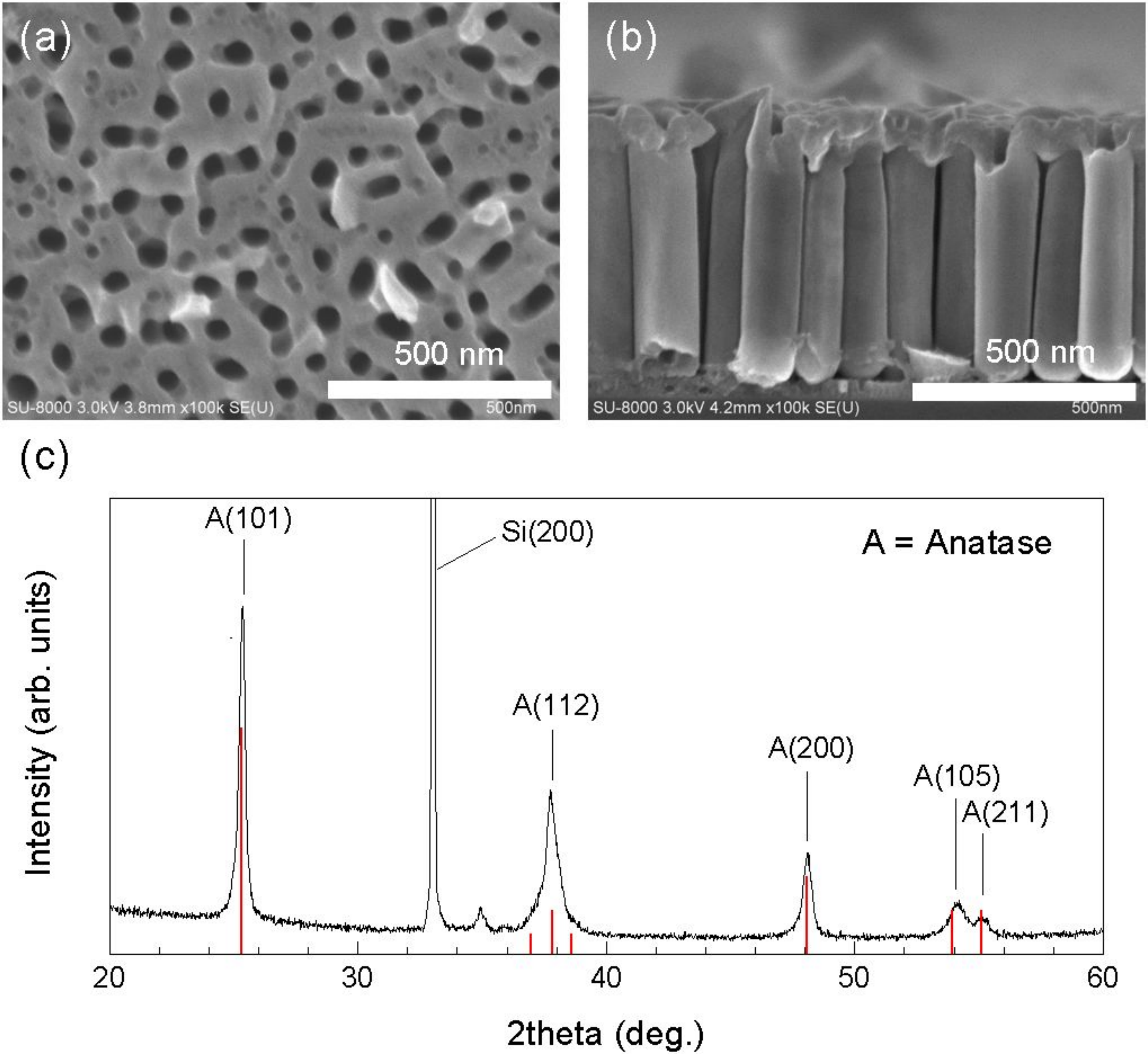
(a)
500 nm
SU-8000 3.0kV 3.8mm x100k SE(U)
500nm
(b)
500 nm
SU-8000 3.0kV 4.2mm x100k SE(U)
500nm
(c)
A(101)
Si(200)
A = Anatase
A(112)
A(200)
A(105)
A(211)
Intensity (arb. units)
20
30
40
50
60
2theta (deg.)

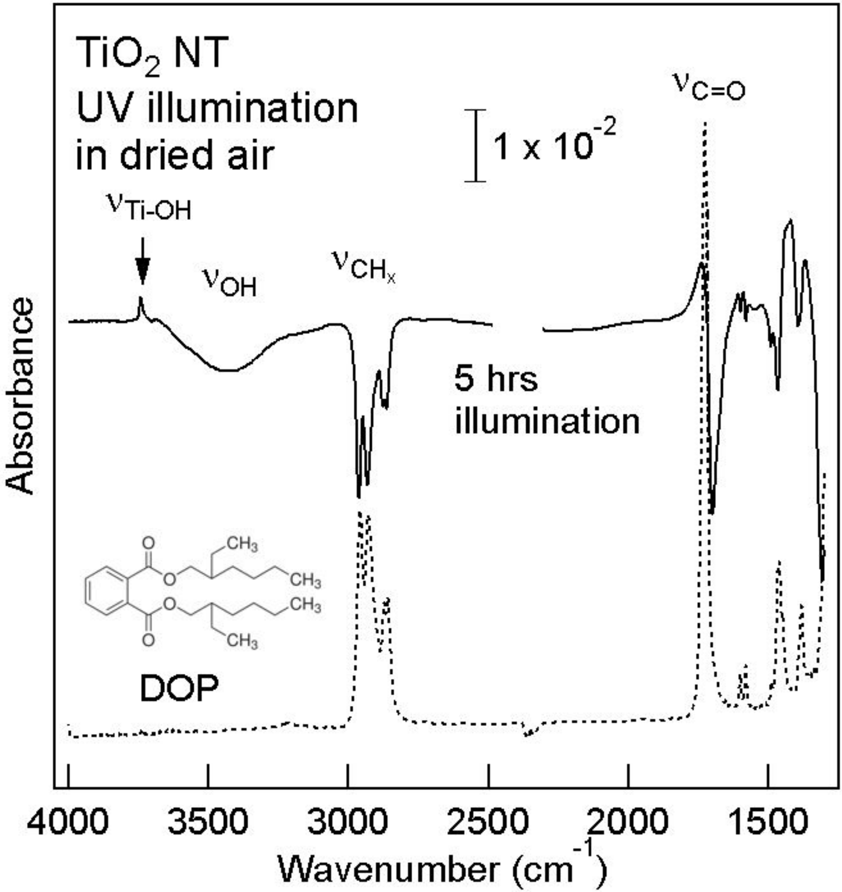
TiO$_2$ NT
UV illumination
in dried air
1 x 10^{-2}
$\nu_{C=O}$
$\nu_{Ti\text{-}OH}$
ν_{OH}
ν_{CH_x}
5 hrs
illumination
CH$_3$
CH$_3$
CH$_3$
CH$_3$
O
O
O
O
DOP
Absorbance
4000
3500
3000
2500
2000
1500
Wavenumber (cm^{-1})

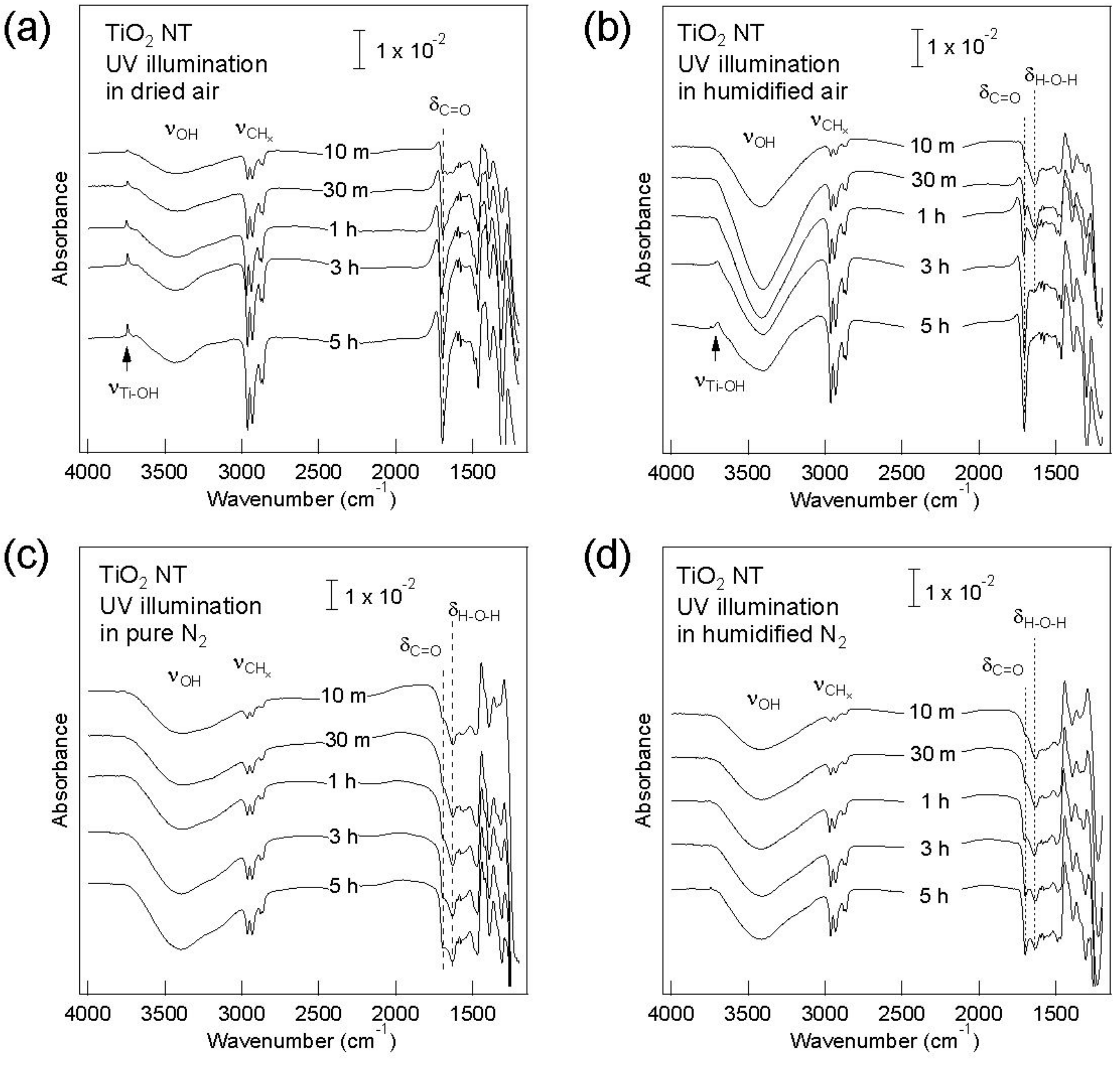
(a)
TiO$_2$ NT
UV illumination
in dried air
1 x 10^{-2}
ν$_{OH}$
ν$_{CH_x}$
δ$_{C=O}$
10 m
30 m
1 h
3 h
5 h
ν$_{Ti-OH}$
Absorbance
4000
3500
3000
2500
2000
1500
Wavenumber (cm^{-1})
(b)
TiO$_2$ NT
UV illumination
in humidified air
1 x 10^{-2}
δ$_{H-O-H}$
δ$_{C=O}$
ν$_{OH}$
ν$_{CH_x}$
10 m
30 m
1 h
3 h
5 h
ν$_{Ti-OH}$
Absorbance
4000
3500
3000
2500
2000
1500
Wavenumber (cm^{-1})
(c)
TiO$_2$ NT
UV illumination
in pure N$_2$
1 x 10^{-2}
δ$_{H-O-H}$
δ$_{C=O}$
ν$_{OH}$
ν$_{CH_x}$
10 m
30 m
1 h
3 h
5 h
Absorbance
4000
3500
3000
2500
2000
1500
Wavenumber (cm^{-1})
(d)
TiO$_2$ NT
UV illumination
in humidified N$_2$
1 x 10^{-2}
δ$_{H-O-H}$
δ$_{C=O}$
ν$_{OH}$
ν$_{CH_x}$
10 m
30 m
1 h
3 h
5 h
Absorbance
4000
3500
3000
2500
2000
1500
Wavenumber (cm^{-1})

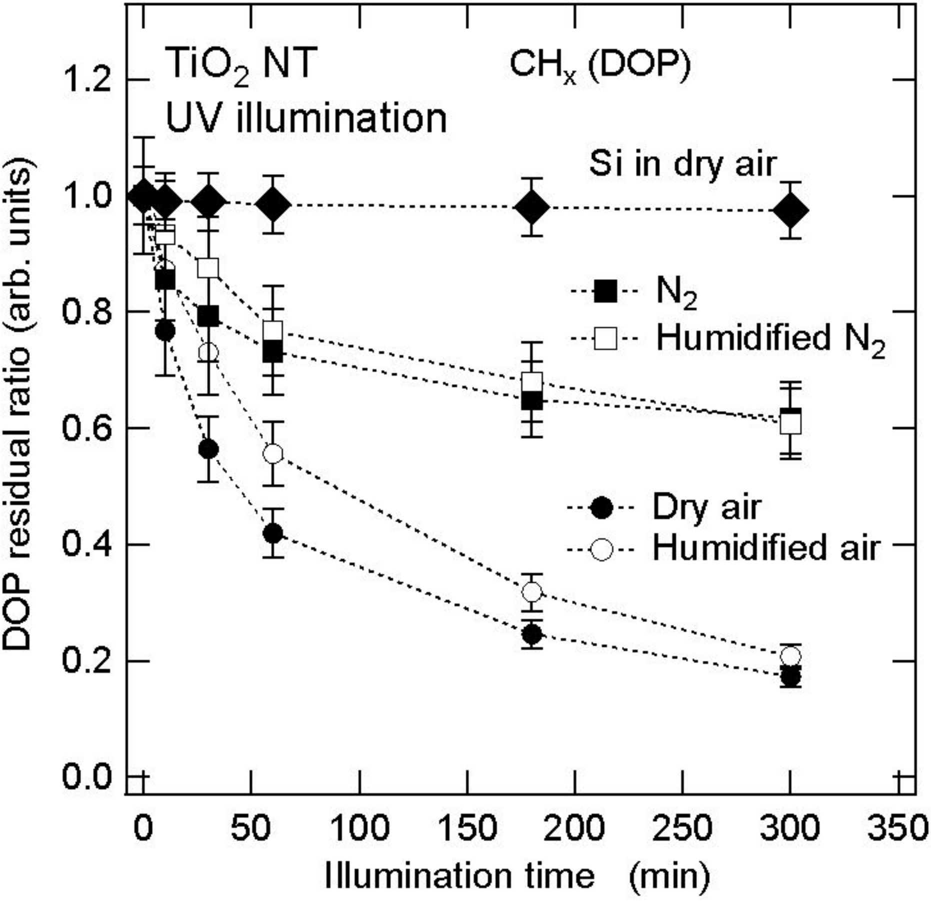
TiO2 NT
UV illumination
CHx (DOP)
Si in dry air
N2
Humidified N2
Dry air
Humidified air
DOP residual ratio (arb. units)
0.0
0.2
0.4
0.6
0.8
1.0
1.2
0
50
100
150
200
250
300
350
Illumination time (min)

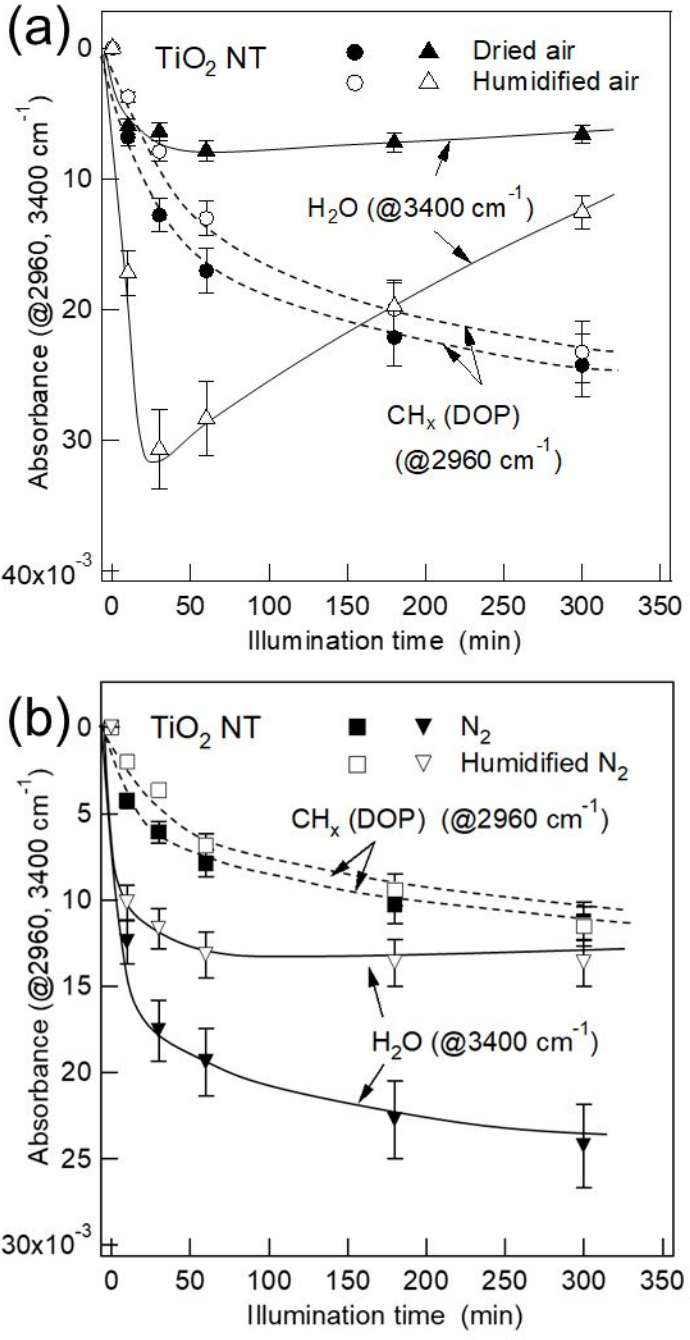
(a)
TiO2 NT
● ▲ Dried air
○ △ Humidified air
H2O (@3400 cm-1)
CHx (DOP)
(@2960 cm-1)
Absorbance (@2960, 3400 cm-1)
0
10
20
30
40x10-3
0
50
100
150
200
250
300
350
Illumination time (min)
(b)
TiO2 NT
■ ▼ N2
□ ▽ Humidified N2
CHx (DOP) (@2960 cm-1)
H2O (@3400 cm-1)
Absorbance (@2960, 3400 cm-1)
0
5
10
15
20
25
30x10-3
0
50
100
150
200
250
300
350
Illumination time (min)

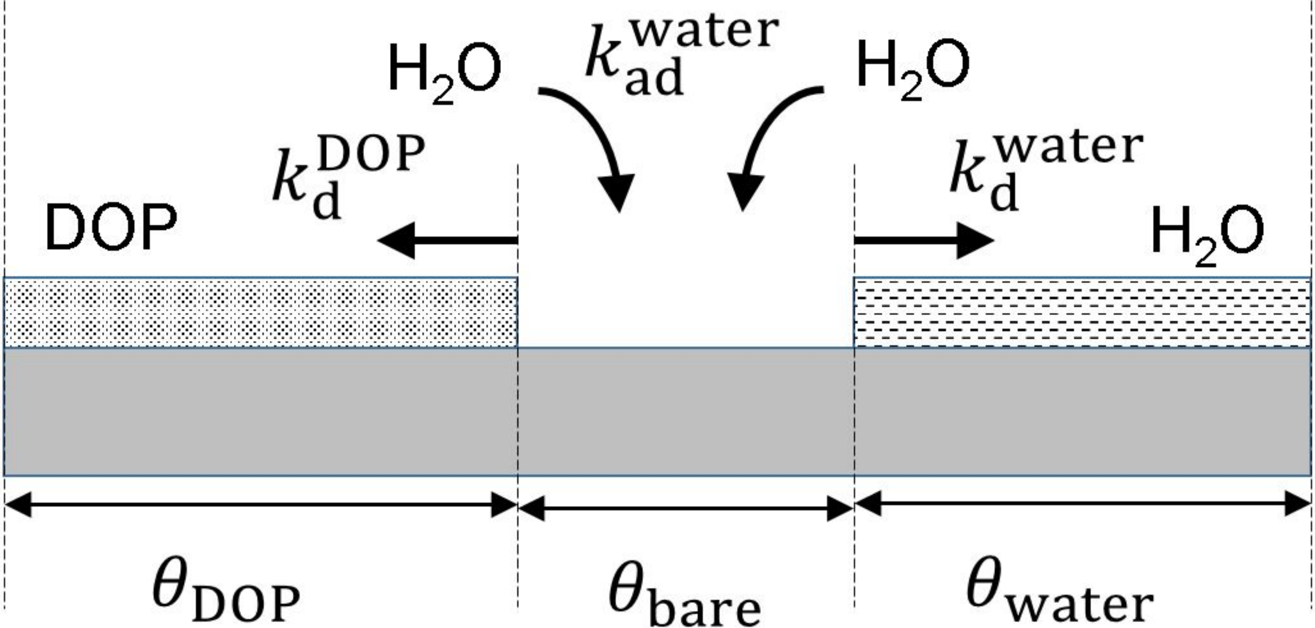

H_2O
$k_{\mathrm{ad}}^{\mathrm{water}}$
H_2O
$k_{\mathrm{d}}^{\mathrm{DOP}}$
$k_{\mathrm{d}}^{\mathrm{water}}$
DOP
H_2O
θ_{DOP}
θ_{bare}
θ_{water}

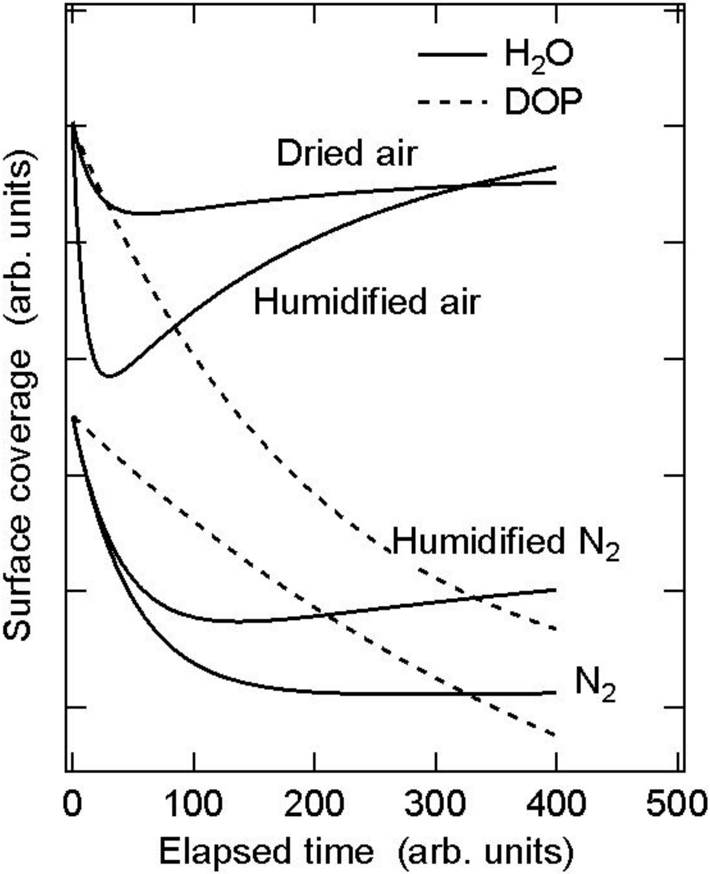
H₂O
DOP
Dried air
Humidified air
Humidified N₂
N₂
Surface coverage (arb. units)
Elapsed time (arb. units)
0
100
200
300
400
500

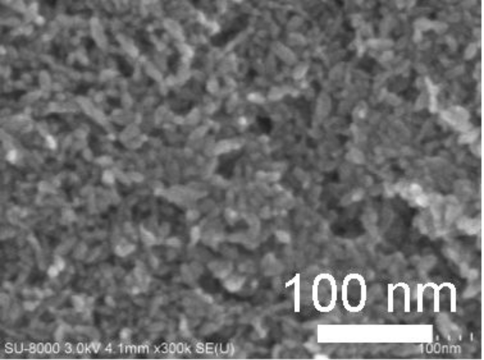
100 nm
SU-8000 3.0kV 4.1mm x300k SE(U)
100nm

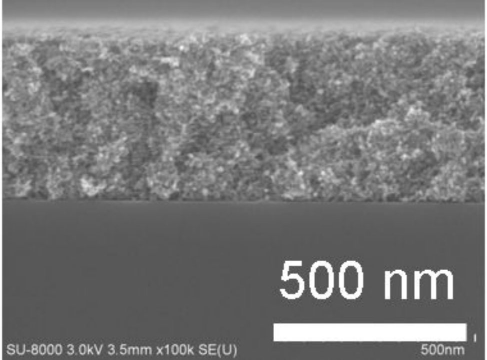
500 nm
SU-8000 3.0kV 3.5mm x100k SE(U)
500nm

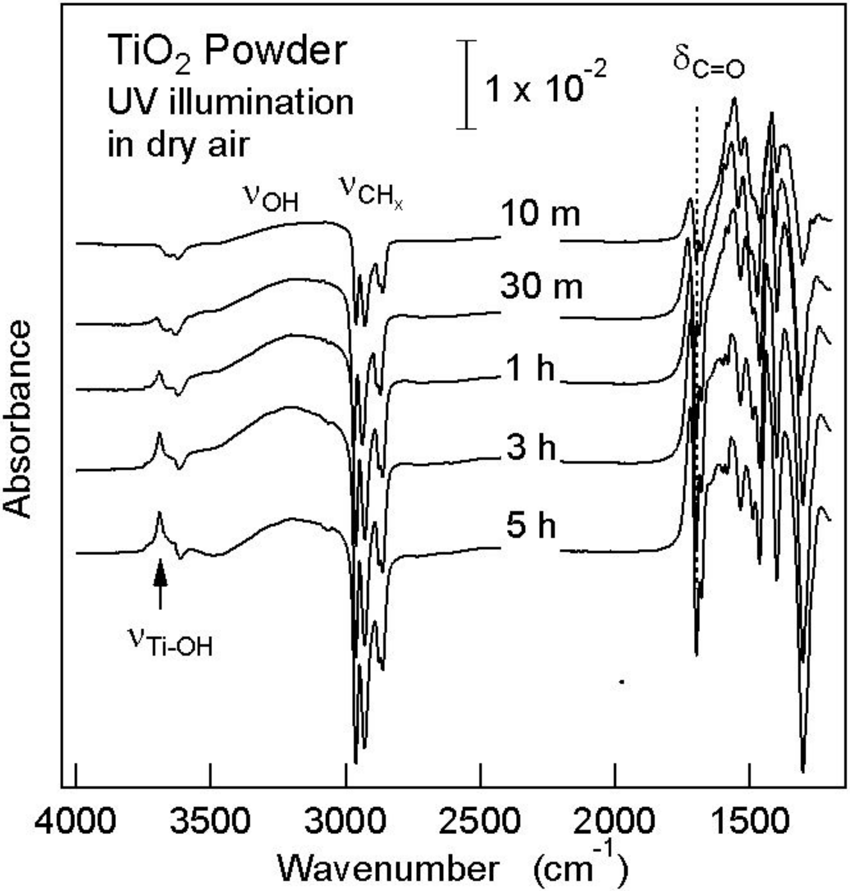
TiO$_2$ Powder
UV illumination
in dry air
1 x 10^{-2}
$\delta_{C=O}$
ν_{OH}
ν_{CH_x}
10 m
30 m
1 h
3 h
5 h
ν_{Ti-OH}
Absorbance
4000
3500
3000
2500
2000
1500
Wavenumber (cm^{-1})

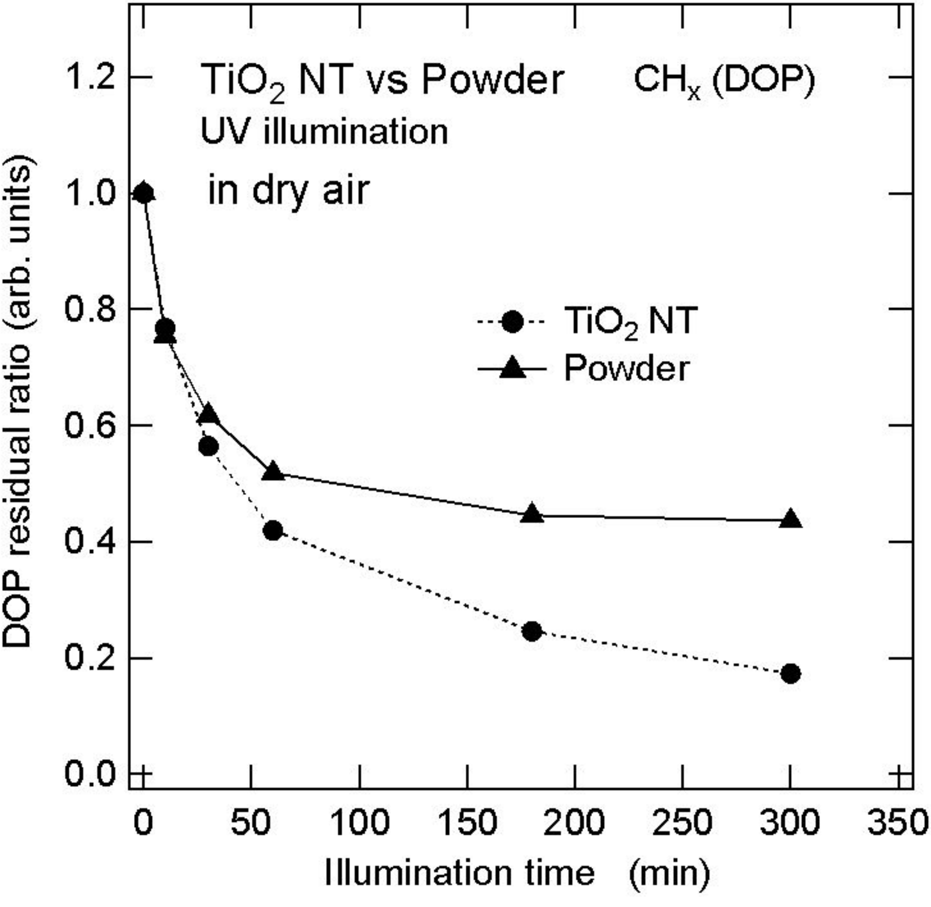
TiO$_2$ NT vs Powder
CH$_x$ (DOP)
UV illumination
in dry air
TiO$_2$ NT
Powder
DOP residual ratio (arb. units)
Illumination time (min)
0.0
0.2
0.4
0.6
0.8
1.0
1.2
0
50
100
150
200
250
300
350